THE JOURNAL OF PHYSICAL CHEMISTRY B

Article

pubs.acs.org/JPCB

Morphology-Dependent Charge Photogeneration in Donor–Acceptor Block Copolymer Films Based on Poly(3-hexylthiophene)-*block*-Poly(perylene bisimide acrylate)

Sven Huettner,[†] Justin M. Hodgkiss,[‡] Michael Sommer,[§] Richard H. Friend,[†] Ullrich Steiner,[†] and Mukundan Thelakkat*[,⊥]

[†]Cavendish Laboratory, University of Cambridge, United Kingdom

[‡]MacDiarmid Institute, Victoria University of Wellington, New Zealand

[§]Institute of Macromolecular Chemistry, University of Freiburg, Germany

[⊥]Applied Functional Polymers, University of Bayreuth, Germany

Supporting Information

ABSTRACT: We have examined how the nanomorphology and crystallinity of semiconducting double-crystalline block copolymers determine their photophysical and photovoltaic responses. The block copolymers consist of a poly(3-hexylthiophene) (P3HT) donor block coupled to a polymerized perylene bisimide acrylate (PPerAcr) acceptor. Different molecular weights and processing solvents allow the modification of the donor–acceptor interface with regard to their morphology and crystallinity. Transient absorption spectroscopy was used to resolve photoinduced charge transfer seen on the ∼1 ps time scale, consistent with substantial photoluminescence quenching caused by finely dispersed, disordered donor–acceptor interfaces. For high molecular weight block copolymers, microphase separation is enhanced by slow film formation, leading to slower charge photogeneration. The crystallinity of the P3HT component is of particular importance, which has been monitored spectroscopically. Crystalline P3HT/PPerAcr interfaces lead to high levels of long-lived charge pairs that are more easily extracted in an applied electric field. While external quantum efficiencies of over 25% were obtained, the overall power conversion efficiency of the best block copolymer device is still limited. This is due to the unsuitable orientation of the block copolymer nanomorphology, and the performance lies below that achieved for a blend of equivalent homopolymers. This suggests that increasing the molecular weight of the block copolymers to tune the microphase separation could further improve the photovoltaic efficiency. Our photophysical results give guidelines for future development of promising block copolymer-derived devices, highlighting the importance of interfacial crystallinity and sufficient phase separation.

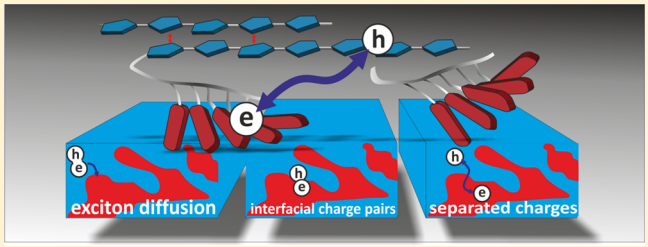

INTRODUCTION

Diblock copolymers offer a platform to realize the conceptually ideal nanoscale morphology for organic photovoltaic (OPV) devices[1] in a single solution processing step. The two segments of a diblock copolymer phase separate during film formation, but due to their covalent linkage, the size of the resulting phases is constrained to the 10 nm length scale. In amorphous block copolymers, self-assembled morphologies ranging from lamellar to cylindrical, gyroidal, and spherical can be obtained, which are determined by the volume ratio of the two blocks.[2] These highly ordered morphologies correspond to their thermodynamic equilibria and offer domain sizes on the order of tens of nanometers, limited by the radius of gyration of the two polymer blocks.[3] In the case where the two blocks are electron donor and acceptor semiconducting materials, the resulting nanostructures can be adjusted to the correct length scale and morphology that govern the efficiency of OPVs, including (i) the exciton diffusion length (∼5–10 nm),[4,5] (ii) the geminate charge capture radius (>15 nm in low dielectric materials),[6] and (iii) the need for bicontinuous networks throughout the active layer for the charges to reach the two electrodes.

We and others have recently reported block copolymer OPVs that combine perylene bisimide acceptor blocks[7,8] and poly(3-hexylthiophene (P3HT) donor blocks.[9−11] P3HT is among the most effective polymers used in OPVs[5,12−14] and organic field effect transistors,[15,16] mainly because of its propensity to form highly crystalline lamellae. Perylene bisimides form crystalline stacks, offering high electron mobilities (up to 2.1 $cm^2/(V\ s)$ in the case of evaporated small molecules[17,18] and 10^{-3} $cm^2/(V\ s)$ in the case of polymerized perylene bisimides[19]). The energy levels of perylene bisimides are suitably positioned to facilitate a

Received: February 28, 2012
Revised: July 2, 2012
Published: July 3, 2012

photovoltaic response when combined with P3HT[20,21] and other conjugated polymers,[22] but the lack of control over the morphology in these blends results in modest photovoltaic efficiencies. Favorable electronic properties of perylene bisimides were recently demonstrated, which can be harnessed in an easily processable form when they are tethered to a polymer backbone.[19,23]

Despite the attractive possibilities of block copolymer OPVs, the best power conversion efficiency achieved to date lies around 2%,[24] substantially lower than in state-of-the-art bulk heterojunction devices using fullerenes (over 8%[25]). Moreover, the photovoltaic response observed for different block copolymer OPVs of similar composition differs widely.[26] This suggests that efficient block copolymer OPVs may only be realized on the basis of an understanding of their photophysical and electronic properties that goes beyond simple conceptual models based on textbook block copolymer nanomorphologies. Crystallinity is one critical parameter, the influence of which is not accounted for in standard block copolymer models. Not only does crystallinity impose a more complex phase behavior on block copolymers,[27] it also determines the photovoltaic response of organic materials which is strongly dependent on the nature and strength of supramolecular interactions and packing.[28] Generally speaking, some degree of crystallinity/order was usually found to favor the device performance. Charge separation efficiencies are found to be remarkably sensitive to the molecular structure at interfaces,[12] yet the diverse assembly processes (phase separation and crystallization) of two different materials inevitably influences interfacial order.

RESULTS AND DISCUSSION

Here, we present a detailed examination of the photovoltaic response and photophysical properties of double crystalline donor−acceptor diblock copolymers. The material (Figure 1) is

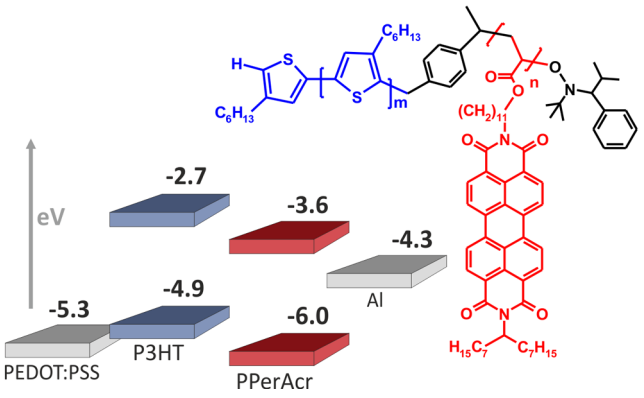

Figure 1. Molecular structure of the investigated donor−acceptor block copolymer P3HT-*b*-PPerAcr consisting of a donor block of poly(hexylthiophene) (P3HT - blue) and poly(perylene bisimide acrylate) (PPerAcr - red) and its HOMO and LUMO levels.[7]

comprised of a P3HT donor block coupled to a poly(perylene bisimide acrylate) (PPerAcr) acceptor block. As summarized in Table 1, BCP1 and BCP2 each contain 45 wt % P3HT and 55 wt % PPerAcr but have differing overall molecular weights (16.7 kg/mol for BCP1 and 29.1 kg/mol for BCP2). For comparison, blends of the corresponding homopolymers were also studied. The synthesis of these materials is presented elsewhere.[29]

Table 1. Molecular Weight and Composition of the Block Copolymers and Blends Determined by GPC (except *)

polymer	total M_n (kg/mol)	weight ratio P3HT/PPerAcr	number of monomers P3HT/PPerAcr
P3HT-*b*-PPerAcr (BCP1)	16.1	44%/56%	27/8
P3HT-*b*-PPerAcr (BCP2)	29.5	45%/55%	51/13
blend P3HT/PPerAcr	~25*/16.6	50%/50%	>100*/20
P3HT-*b*-PPerAcr (BCP3)	24.8	19%/81%	27/19

Employing block copolymers with two different molecular weights, combined with different film preparation routes, allows us to widely vary the crystallinity and interfacial structure. By employing a combination of structural, photophysical, and electronic measurements for films and devices prepared from P3HT-*b*-PPerAcr block copolymers, we are able to elucidate the parameters required to be controlled in donor−acceptor block copolymer devices.

Figure 2a shows the normalized absorption spectra of the P3HT and PPerAcr homopolymers and the BCP2 block copolymer in thin films. Since both BCP 1 and BCP 2 exhibit identical absorption spectra, only the BCP 2 spectrum is shown here. P3HT exhibits a well-resolved vibronic structure with significant intensity in the 0−0 band at 610 nm. This feature is associated with planarized chains which allow crystallization in a lamellar structure[30] and interchain delocalization of the excitons.[31] Therefore, this feature is a clear indication for the prevalence of crystalline packing of P3HT chains. PPerAcr contains side chains consisting of perylene bisimide moieties that are connected to the poly(acrylate) backbone via an alkyl spacer. The flat perylene bisimide cores have strong $\pi-\pi$ interactions. The coupling of the π orbitals leads to a mixing of Frenkel excitons with charge transfer excitons.[32] Enhanced aggregation of the perylene bisimide leads to a relative increase of the feature at 465 nm, as well as in the low energy tail at approximately 580 nm.

The absorption spectra of block copolymer series can be approximated by a linear combination of the two homopolymer spectra weighted by their molecular weight ratios (see the Supporting Information). The divergence of block copolymer absorption spectra from the linear combination of homopolymers is most pronounced in the 610 nm region and is clearly dependent on film preparation. Since the intensity of the 610 nm peak is a signature of P3HT crystallinity (vide supra), we find that crystallinity is markedly suppressed when the block copolymer film forms rapidly (via spin-coating from the low boiling point solvent chloroform (CF) ($T_{B.P.}$ = 61 °C). On the other hand, film formation is sufficiently slow when cast from chlorobenzene (CB) ($T_{B.P.}$ = 131 °C), and here a high level of crystallinity is achieved within the P3HT phase. In a similar manner, it is possible to recover the P3HT crystallinity by subsequent solvent vapor annealing or temperature annealing steps (data not shown).[33] As optimized during previous work,[9] CB serves as the best solvent for these devices and is therefore used as a reference in the following.

We have reported elsewhere that P3HT and PPerAcr domains consist of two coexisting crystalline regions with hierarchical structures that are driven by strong $\pi-\pi$ stacking, as shown by X-ray scattering.[33] The perylene bisimide moieties form one-dimensional π stacks which assemble into an oblique

dx.doi.org/10.1021/jp301966p | J. Phys. Chem. B 2012, 116, 10070−10078

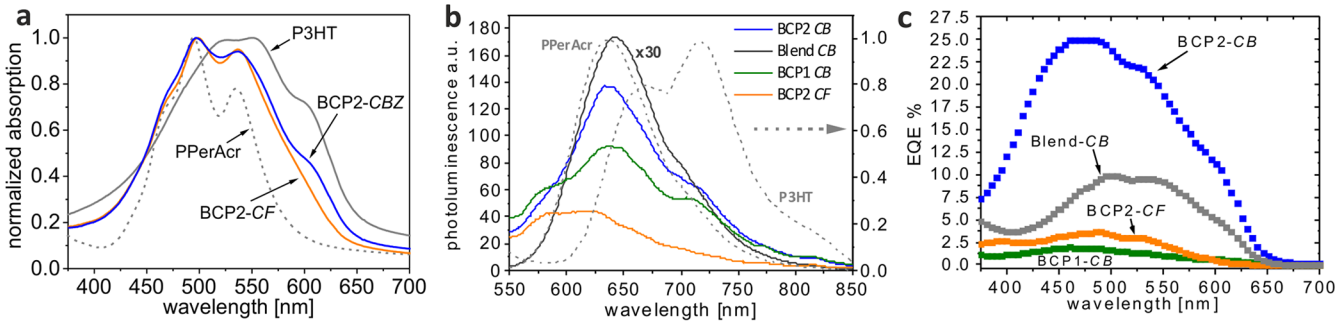

Figure 2. (a) Absorption spectra of the used materials. The BCP2 spectra are equivalent to a linear superposition of the homopolymer spectra with P3HT:PPerAcr ratio of 48−52%. The P3HT crystallinity is strongly reduced in the BCP2 block copolymer when spin-coated from chloroform, as seen from the decrease in the 610 nm feature. (b) Photoluminescence (PL) spectra excited at 490 nm. The blend is scaled by a factor of 30. The PPerAcr and P3HT homopolymers (gray, dotted) are shown on a normalized scale. (c) Current-action spectra of the tested material composites measured under short circuit conditions.

Table 2. Device Parameters of Photovoltaic Device Measurements: Open Circuit Voltage V_{OC}, Short Circuit Current J_{sc}, Fill Factor FF, Power Conversion Efficiency η, External Quantum Efficiency EQE, Photolumincescence Quantum Efficiency PLQE from Quantitative Fluorescence Measurements, and Hole Mobilities μ_h Estimated from Hole Only Devices Using the Space Charge Limited Current (SCLC) Equation

device	V_{OC}	J_{SC}	FF	η	PLQE	EQE_{max}	μ_h (SCLC)
BCP 2 *chloroform*	0.50	0.03	0.20	0.003%	0.71%	3.6%	10^{-10} cm^2/(V s)
BCP 2 *chlorobenzene*	0.42	1.56	0.30	0.20%	1.19%	25%	10^{-6} cm^2/(V s)
BCP 1 *chlorobenzene*	0.51	0.07	0.17	0.007%	0.76%	2%	10^{-8} cm^2/(V s)
blend *chlorobenzene*	0.56	1.25	0.49	0.35%	6.85%	10%	10^{-6} cm^2/(V s)
BCP 3 *chloroform*	0.58	0.007	0.24	0.0009%		0.8%	

two-dimensional lattice exhibiting liquid crystalline order. P3HT forms crystalline lamellae. The crystallization of both blocks has a significant effect on the phase separation of the block copolymer, as the estimated order−disorder transition temperature of the block copolymer phase separation is below the crystallization temperature. Consequently, the crystallization of the blocks induces a microphase structure (depending on the molecular weight) with a domain spacing of around 15 nm in the bulk, irrespective of the block ratio. This structure does, however, not necessarily reflect the phase morphology immediately after spin-coating or a short annealing step, nor does it reflect the energy landscape that gives rise to most optical excitations. In the following sections, we refine the model of the P3HT-*b*-PPerAcr copolymer morphology based on photophysical and photovoltaic measurements.

Strong optical absorption arising from both PPerAcr and P3HT chromophores (Figure 2a) leads to exciton photogeneration in both phases. When intrachain excitons diffuse to a donor−acceptor interface, the energy level offset across the heterojunction induces the formation of nonemissive interfacial charge transfer states and ultimately free charge carriers. As a consequence, the photoluminescence quantum efficiency (PLQE) is strongly quenched in films of the block copolymers compared to the individual homopolymers (PLQE (P3HT) ≈ 4%,[34] PLQE (PPerAcr) ≈ 20%, see Table 2). Films of BCP2 spin-coated from CB result in a PLQE of only 1%, and the CF processed films are even lower at 0.8%. The lower molecular weight block copolymer BCP1-CB has a barely quantifiable PLQE of less than 0.1% (Table 2). Strong PLQE quenching in the block copolymers illustrates that donor−acceptor interfaces are assembled on length scales considerably shorter than the exciton diffusion lengths of the individual materials (Figure 2b). The analysis of PL quenching highlights the particularly finely interspersed donor−acceptor morphology that results in films that dry rapidly (cast from CF) and films comprised of the low molecular weight block copolymer (BCP1). The PLQE recovers to around 7% in the blend of homopolymers cast from CB, confirming the much coarser donor−acceptor morphology that results from the macrophase separation in blends.

Quantitative analysis of PL quenching must be balanced by consideration of the respective composition. The PL spectra of block copolymer films are dominated by PPerAcr emission (λ_{max} = 636 nm) with a minor contribution of P3HT emission (λ_{max} = 716 nm) (Figure 2b). A broad feature at 580 nm seems to be always present in BCP. Because of a comparable spectral PL signature in P3HT solutions, we attribute this feature to amorphous P3HT chains.[35] Efficient resonant energy transfer is typically dominated by emission from the lowest energy chromophore, in this case ordered regions of P3HT. Emission from disordered P3HT chains is not usually detectable in solid films of P3HT for this reason.[31] Thus, the PL spectra suggest that excitons are frequently generated on PPerAcr and disordered P3HT chains that are too isolated to transfer energy to ordered P3HT domains. Second, the higher inherent PLQEs of PPerAcr and disordered P3HT chromophores compared to ordered P3HT further enhances their relative contribution to PL.[36] Notwithstanding, the high levels of PL quenching in all cases points to high yields of charge photogeneration.

Despite the higher yields of charge generation seen for finely distributed donor−acceptor interfaces, the quantum efficiency of subsequent charge extraction is known to favor somewhat coarser morphologies where the geminate charge pairs are able to escape their mutual Coulomb attraction.[6] Figure 2c shows the external quantum efficiency (EQE) plot of photovoltaic devices with active layers comprised of block copolymers of two different molecular weights, and each processed from both low-

dx.doi.org/10.1021/jp301966p | J. Phys. Chem. B 2012, 116, 10070−10078

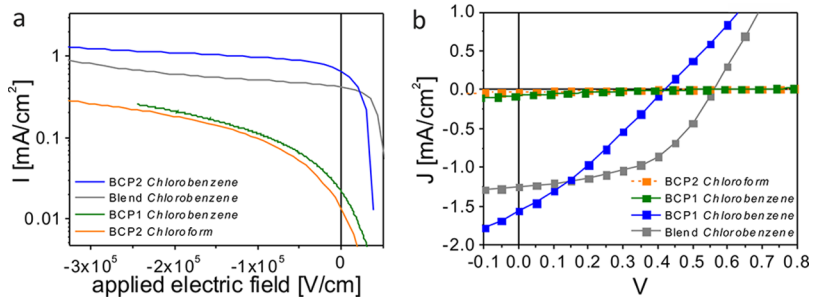

Figure 3. (a) $J-V$ characteristics under low intensity illumination and an externally applied electric field additional to the built-in potential, which can be roughly estimated to 7×10^4 V/cm. The bias is converted into the electric field applied at the film. Charge pairs generated in BCP1-CB and BCP2-CF are only extracted with the help of an electric field, so that the current increases by 1 order of magnitude before it starts to saturate. The blend and the BCP2-CB device instead show efficient charge extraction already at zero applied field (i.e., under short circuit conditions). (b) $J-V$ characteristics of organic photovoltaic devices tested under simulated sunlight at AM1.5 at 100 mW/cm^2.

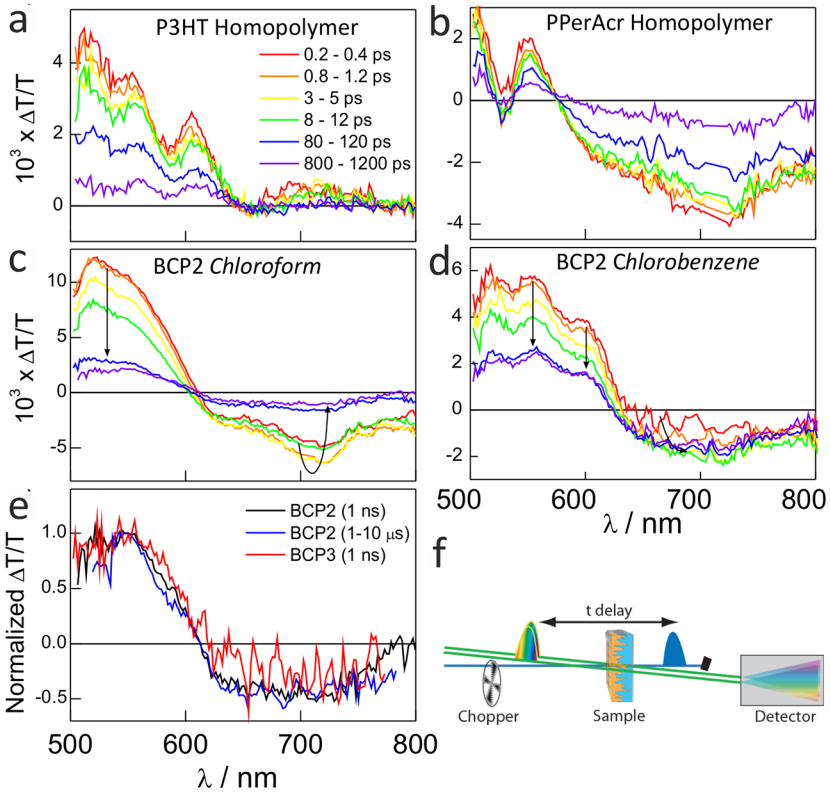

Figure 4. Time evolution of transient absorption (TA) spectra in thin films of (a) P3HT homopolymer, (b) PPerAcr homopolymer, (c) BCP2-CF, and (d) BCP2-CB. The same time ranges are integrated in each case according to the color scheme shown in part a. (e) Normalized TA spectra for thin films of the BCP2 diblock copolymer at probe delays of 1 ns and 1−10 μs, along with the BCP3 (81% PPerAcr) diblock compolymer at a probe delay of 1 ns. A 490 nm, 60 fs pulsed excitation with a fluence of (2−4) $\times 10^{14}$ photons/cm^2 was used to obtain all spectra except the μs time scale spectra, which employed 532 nm, 600 ps excitation at the same fluence (see the Experimental Section for details). (f) Schematic of the TA setup.

and high boiling point solvents. Devices with an active layer processed from chloroform reach EQEs of only 2 and 3.6% for BCP1-CB and BCP2-CF, respectively. As described previously,[9] maximum EQEs of over 25% have been achieved using BCP2 with a high molecular weight P3HT block, spin-coated from CB. A blend of the two constituent homopolymers results in a peak EQE of around 10% when processed under the same conditions. The superior EQE found when using this block copolymer demonstrates the success in achieving an optimal balance of exciton-to-charge conversion and charge extraction by controlling the nanomorphology of the photoactive layer.

The EQE values stated above were determined under short circuit conditions. Application of a large negative bias assists the field-induced separation of interfacial charge pairs and provides sufficient driving force for the extraction of charges that would otherwise remain trapped at interfaces, particularly in films with a high interfacial area. Figure 3a shows the field dependence of the photocurrent measured under low light intensity (28 mW/cm^2) to avoid second-order effects like bimolecular charge recombination. The chloroform processed device (BCP2-CF) exhibits a much lower short circuit current J_{sc} compared to BCP2-CB. Upon application of a strong reverse bias, the photocurrent increases by 1 order of magnitude, highlighting the charge population that is lost under short-circuit conditions to geminate recombination in the chloroform processed device.[37] On the other hand, in the BCP2-CB or homopolymer

dx.doi.org/10.1021/jp301966p | J. Phys. Chem. B 2012, 116, 10070−10078

blend devices, the photocurrent is already close to saturation under short-circuit conditions. Photoconductivity may also contribute to the apparent photocurrent at high reverse bias.[38]

Figure 3b shows the corresponding $J-V$ curves measured under AM1.5 100 mW/cm^2 simulated solar illumination, and Table 2 lists the analyzed device parameters. Despite its superior short-circuit photocurrent, BCP2-CB devices have a reduced fill factor (FF) and open circuit voltage (V_{OC}) compared with the homopolymer blend, and an overall power conversion efficiency of only η = 0.20%, compared with η = 0.35% for the blend. The BCP2-CF or BCP1-CB devices exhibit substantially lower power conversion efficiencies of η = 0.003 and η = 0.007%, respectively. The observed trend in PCEs is correlated with the degree of P3HT crystallinity and inversely correlated with the interfacial area which is inferred from UV−visible absorption and PL measurements.

The morphology dependence of photocurrent extraction is supported by the analysis of charge mobilities in the various devices. Substituting the aluminum cathodes for higher workfunction gold contacts turns the devices into hole-only diodes and permits one to estimate hole mobilities by fitting the space-charge limited currents[39] (see the Supporting Information). The BCP2-CB devices show estimated hole mobilities of around 10^{-6} cm^2/(V s). The hole mobilty is reduced by 2 orders of magnitude for BCP1-CB (10^{-8}cm^2/(V s)), consistent with the trends observed for the same materials incorporated in OFET devices.[9] The hole mobilty of BCP2-CF devices is reduced by 4 orders of magnitude to 10^{-10} cm^2/(V s). Such a large difference is not usually observed in OFET devices, highlighting the role of the bulk film morphology influencing the charge mobility.

The observed reduction in charge mobility for the various block copolymer devices reflects the coupled effects of the increased interfacial area and the reduced crystallinity. The crystallinity of P3HT is already known to play a crucial role in block copolymer OPV devices[9] and P3HT/fullerene blend devices,[40] with highly crystalline structures resulting in high hole mobilities. This is usually achieved in high molecular weight range P3HT by processing in high boiling point solvents such as CB or by thermal annealing. Importantly, it is the local charge mobility caused by P3HT crystallinity in the vicinity of heterojunction interfaces that is expected to have the biggest effect on charge separation.[36] While the series of absorption spectra clearly demonstrates that overall P3HT crystallinity is strongly affected by the interfacial area, absorption spectroscopy or X-ray scattering does not distinguish between chains at interfaces and in the bulk.

By employing transient absorption (TA) spectroscopy as a direct probe of the nature and dynamics of photoexcitations generated in films of diblock copolymers under different processing conditions, we are able to directly interrogate the formation and properties of interfacial states, including those caused by the crystallinity of interfacial polymer chains. A schematic of the experiment is shown in Figure 4f. Figure 4a and b shows the TA dynamics for the two homopolymers in order to establish the spectral properties and dynamics in the absence of donor−acceptor heterojunctions for charge separation. In the case of P3HT spin-coated from chlorobenzene (Figure 4a), the series of TA spectra are dominated by bleaching ($\Delta T/T > 0$) of the ground-state (GS) absorption at λ < 650 nm. Accordingly, a vibronic progression is clearly resolved in the ground-state bleaching (GSB) signal. The prominence of the 0−0 band at 610 nm shows that excitations occupy P3HT chains which adopt a planar chain conformation and are packed in order. The positive $\Delta T/T$ signal in the λ = 650−750 nm region coincides with the weak P3HT photoluminescence and is thus attributed to stimulated emission (SE) from P3HT excitons. No photoinduced absorption (PIA) ($\Delta T/T < 0$) is seen for the probed wavelength range. The P3HT signal exhibits a nonexponential decay with a half-life of ∼100 ps, and the bleaching features display a dynamic red-shift as excitons migrate toward more extended chains and delocalize.

In the case of PPerAcr, the spectra are dominated by a broad PIA signal at λ_{max} = 720 nm, with a sharp GSB feature at λ = 550 nm and further bleaching at the blue edge of the spectrum. These features are consistent with aggregated PPerAcr chromophores,[41] and the spectrum decays dispersively with a half-life of ∼100 ps.

Figure 4c shows the TA dynamics for a BCP2-CF film. The earliest TA spectrum (200−400 fs, red curve) exhibits GS bleaching at λ < 600 nm and an absorption feature centered at 720 nm, each of which are distinct excitonic features of the constituent P3HT and PPerAcr homopolymers. The strong 490 nm absorption by both chromophores (48% P3HT and 52% PPerAcr, see the Supporting Information) suggests that the copolymer TA spectrum might be approximated by the weighted sum of the homopolymer spectra. In contrast to the homopolymer TA spectra, however, the diblock copolymer BCP2-CF clearly lacks vibronic structure in the P3HT GS bleaching region. Specifically, the lack of bleaching intensity in the 0−0 band at 610 nm is consistent with our conclusion from UV−vis absorption and PL spectroscopy that the PPerAcr block disrupts P3HT chain planarity and lamellar packing. Within the next picosecond (orange curve), the TA spectrum of the diblock copolymer is seen to enhance its PIA intensity beyond 620 nm, while the GS bleaching region remains unchanged. By comparison to the homopolymer reference spectra, an energy transfer process dominating the early time spectral evolution can be ruled out by considering each of the possible energy transfer processes: (i) energy transfer from P3HT* to PPerAcr would be associated with *decreased* GS bleaching at λ < 600 nm on a commensurate time scale with an *increased* photoinduced absorption beyond 620 nm, and (ii) energy transfer from PPerAcr* to P3HT would lead to *increased* GS bleaching at λ < 600 nm and *decreased* photoinduced absorption beyond 620 nm. Instead, we attribute the spectral dynamics on the 1 ps time scale to the conversion of P3HT-based excitons to interfacial charge pairs. Through this process, the P3HT GS bleach is retained, while a rather flat PIA feature beyond 620 nm appears from a combination of electrons in PPerAcr and holes in P3HT, consistent with previous TA studies of charges in these materials.[42,43] Charge generation could also proceed via PPerAcr excitons. If this was the dominant mechanism, an *increase* in the P3HT-based GS bleach concomitantly with charge generation would be expected. There appears to be a population of PPerAcr excitons still present on slightly longer time scales, based on the survival of the 720 nm PIA peak in the 8−12 ps spectrum. This observation is consistent with the traces of PPerAcr emission seen in PL spectra (Figure 3a). Combinations of energy transfer processes preceding a much faster charge transfer step are also likely to occur, but if the intermediates are short-lived, this mechanism is spectroscopically indistinguishable from direct charge generation. Thus, a major contribution to charge generation arises via P3HT excitons. The assignment of charge

pair formation is supported by the comparison of the various normalized TA spectra shown in Figure 4e. The close resemblance of TA spectra for diblock copolymers with vastly different ratios of the P3HT and PPerAcr (PPerAcr content varying from 55 to 81%; BCP3-only TA data shown here, photovoltaic performance is 1 order of magnitude lower than BCP2-CB), is consistent with an interfacial state rather than a mixture of states localized in each domain type. Moreover, the survival of the TA spectral features on the microsecond time scale is consistent with charges and not singlet excitons. Finally, the detection of photogenerated charges is quantitatively consistent with our photocurrent measurements. On the basis of the magnitude of the GS bleach at 1 ns compared with the initial signal at 300 fs, we constrain the yield of excitations that could contribute to photocurrent to <20%. The corresponding chloroform-processed OPV devices have a peak short-circuit external quantum efficiency of 3.6% (Figure 2c) (and higher under reverse bias), suggesting that most if not all of the excitations detected beyond the disappearance of excitons must be charges. This also suggests that triplet excitons do not play a significant role. Triplets have been demonstrated to form in high yields via recombination of interfacial charge-transfer states in blends where this is thermodynamically favorable.[44−46] In the case of P3HT-*b*-PPerAcr, the interfacial charge transfer state is estimated to be close in energy to triplet excitons in P3HT, based on an estimated driving force of 0.6 eV[47] for charge transfer from the P3HT singlet exciton compared with the range of exchange energies found for ordered P3HT (0.45 eV)[48] and an extensive range of amorphous conjugated polymers (0.7 eV).[49]

The spectral signatures in Figure 4 can also be used to resolve the time scale of charge transfer. The population of charge pairs peaks within only 3 ps for the chloroform-processed film, as ascertained from the growth of the PIA signal at 700 nm. This fast time scale is consistent with the substantial PL quenching and reflects a finely interdispersed phase morphology. This observation may seem at odds with the ∼10 nm radius of gyration of the block copolymer segments. This discrepancy is reconciled by the assumption of incomplete phase separation caused by rapid film drying when cast from CF. This interpretation is consistent with other investigations on the dependence of film drying time on phase separation, and with the spectroscopic observation that P3HT chains are disordered in the BCP2-CF films.[36]

Figure 4d shows the evolution of TA spectra for a film of BCP2 processed from CB and measured under identical conditions as the film of BCP2-CF. There are several striking differences in the TA spectral evolution. The prominence of the GS bleach of the 0−0 vibronic peak at 610 nm is clear evidence that excitations occupy crystalline P3HT domains, which corresponds to the changes in the UV−vis absorption spectrum. Whereas UV−visible absorption spectroscopy measures the average P3HT crystallinity in the film, TA spectroscopy can yield information about crystalline ordering in the vicinity of interfaces where charges are formed. The retention of the 610 nm GSB peak beyond the time scale of charge generation shows that interfaces occupied by charge pairs are considerably better ordered when films are cast from CBZ than from CF. The TA spectra support our previous assertion that enhanced interfacial ordering plays a crucial role in facilitating the initial separation of charge pairs and accounts for considerably higher photovoltaic efficiencies observed when a higher molecular weight polymer is processed from chlorobenzene (i.e., BCP2-CB).

Figure 5a compares the rate of charge generation, as assessed from the growth of the photoinduced absorption feature at

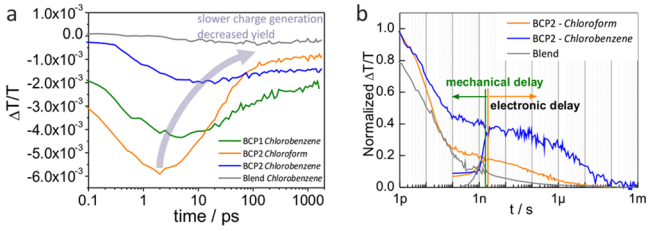

Figure 5. (a) Charge generation kinetics probed in the photoinduced absorption region (λ_{probe} = 700−750 nm) for BCP1 and BCP2 as well as for the P3HT/PPerAcr blend. The coarser the donor−acceptor interface, the slower the generation of charge at the interface, causing a decrease in their overall number. An efficient charge separation is, however, only given at sufficiently coarse domains with an increased P3HT crystallinity. (b) Normalized TA kinetics in the GS bleach region (λ_{probe} = 530−570 nm) for thin BCP2 films cast from chloroform (orange curve) and CB (blue curve) on time scales of 1 ps to 1 ms, following pulsed excitation as well for the blend spin-coated from chlorobenzene (gray curve). This plot was obtained by splicing the normalized kinetics obtained on sub-ns time scales (using mechanically delayed 60 fs pulses) and > ns time scales (with electronically delayed 600 ps excitation pulses).

700−750 nm in the time scale of 0.1−1000 ps, for each of the block copolymers spin-coated from different solvents and for the blend of homopolymers. A clear trend is observed: the charge population peaks at later times for CB processed films compared with those processed from CF, and likewise for high vs low molecular weight block copolymers. The peak charge population is still later in the blend of homopolymers. Since excitons must diffuse to an interface prior to generating charges, a slower rate of charge generation is consistent with a coarser phase separation and purer phase compositions adjacent to the interfaces.[36] A similar trend is observed in the magnitude of the peak charge population, with earlier absorption peaks being associated with higher yields of charge generation, consistent with PLQE trends. We note that exciton-charge annihilation can also operate to complicate the quantitative analysis of charge generation kinetics at this excitation density.[50] Consistent with the GSB kinetics, only ∼20% of the maximum charge population (peaked at ∼2 ps) is found to survive beyond 100 ps in the chloroform-processed film, suggesting that geminate charge recombination proceeds rapidly across the disordered interfaces of chloroform-processed block copolymer films. Subnanosecond geminate charge recombination has recently been identified as limiting the efficiency of some donor−acceptor blends that do not include fullerenes.[51]

The comparison of the TA dynamics in the GS bleaching regions reveals that P3HT crystallization is also associated with a significantly higher level of charges surviving beyond the nanosecond time scale. We were able to resolve the dynamics of charge recombination on longer time scales by synchronizing a *Q*-switched Nd:YVO_4 excitation laser with the femtosecond probe via an electronic delay generator. Figure 5b shows the normalized GS recovery kinetics for BCP2 and homopolymer-blend films processed from CF and CB. Excitation kinetics measured with mechanical and electronic delays are spliced together to give a gap-free time range from 1 ps to 1 ms. The BCP2 cast from CB clearly has a higher population (>40% of

dx.doi.org/10.1021/jp301966p | *J. Phys. Chem. B* 2012, 116, 10070−10078

initial excitations) of charges that decay very little between 100 ps and 1 μs, providing an extended time window for charge pairs to separate in the device. The ~25% peak EQE measured for the corresponding BCP2-CB device is clear evidence that most of the interfacial charge pairs observed at 100 ps are subsequently effectively separated and extracted from the device at short circuit.

Figure 6 shows the schematic thin film morphologies deduced from steady state and transient absorption spectroscopy. From the TA data, we infer domain sizes well below, around, and well above the exciton diffusion length for BCP1-CB, BCP2-CB, and the homopolymer blend, respectively. Scanning electron microscopy (SEM) of these films was carried out to correlate the excitation kinetics with the polymer morphology. The block copolymer films indeed suggest that morphologies of different coarsenesses are present. The blend film clearly displays large macroscopic domains, whereas the domain sizes in BCP films are at the limit of resolution. These results further confirm the conclusions drawn from TA spectroscopy, which is capable of elucidating indirectly the fine morphological influences on charge separation.

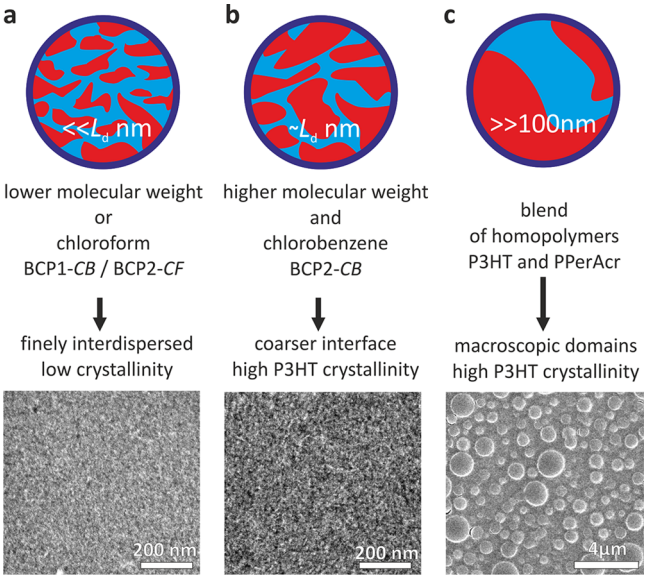

Figure 6. Schematics of attributed morphologies achieved by processing homo- and block copolymers from different solutions and corresponding scanning electron microscopy images. Parts a and b depict the block copolymers. The morphology is too small to be properly resolved by SEM. The domain size is deduced from spectroscopic data, estimating a finely interdispersed morphology much smaller than the exciton diffusion length L_D (a) and on the order of the exciton diffusion length (b). The blend demixes on a micrometer length scale (c).

CONCLUSION

In conclusion, we have investigated the kinetics of charge generation in donor−acceptor block copolymer systems of P3HT-*b*-PPerAcr. Since block copolymer phase separation is induced by the crystallization of the individual blocks, the use of different solvents and molecular weights permits the variation of domain sizes (i.e., interfacial coarseness) and interfacial P3HT crystallinity.

The measured charge generation time scales are below $t_{1/2}$ = 1.5 ps, and there is considerable kinetic redundancy in the rate of charge generation for all block copolymer films when comparing to the exciton lifetime ($t_{1/2}$ ~ 100 ps). Such rapid charge generation implies that donor−acceptor interfaces are effectively distributed at a distance of just a few nanometers, significantly below the ~15 nm length scale of copolymer microphase separation measured by X-ray scattering in the bulk. This difference in length scales in as-cast films suggests that donor and acceptor blocks have not fully reached the predicted equilibrium mircophase morphology. Rough interfaces and disrupted crystallinity impedes the separation of geminate charge pairs, resulting in the rapid and substantial charge recombination seen in TA measurements and PV response curves.

The fine donor−acceptor interdispersion is also confirmed by the strongly quenched photoluminescence. Interfacial P3HT crystallinity is important for efficient charge separation as the charge carrier mobility and the domain size are correlated. Low boiling point solvents such as CB and a sufficiently high molecular weight of the P3HT block (here M_n = 17.0 kg/mol) enhance P3HT crystallinity. The increase in molecular weight may also favor microphase separation. BCP2-CB has therefore the highest external quantum efficiency, which is strongly correlated with high populations of long-lived charges occupying interfacial crystalline regions from which they can be easily extracted. However, the morphology for complete charge separation and extraction still leaves considerable room for improvement. In a highly phase separated blend of the two homopolymers, for example, the fill-factor is 20% higher than in the best block copolymer device and the open circuit voltage is increased by 0.18 V, despite the much reduced generation of photogenerated charges compared to BCP2. The blend with its macrophase separation still outperforms the BCP2 device under higher light intensity, further indicating the importance of pure percolation pathways in order to reduce geminate recombination and to increase the fill-factor as well as V_{OC}. The domain size, phase separation into pure phases, and the desired structural orientation in microphase separated block copolymers may have to be further tuned to exploit the advantages of these systems. One big challenge may be to obtain block copolymers which show microphase separation in the molten state, which on cooling give rise to pure crystalline domains. Our results suggest that diblock copolymers with a much higher molecular weight should result in morphologies that produce even more efficient OPV devices. The use of BCPs as interfacial compatibilizers in a blend[52] of homopolymers offers an alternative strategy that could provide larger pure phases and well-defined crystalline interfaces to improve device performance.

EXPERIMENTAL SECTION

Sample Preparation and Characterization. The synthesis of PPerAcr and PPerAcr-containing block copolymers has been described elsewhere.[29] The P3HT homopolymer was purchased from *Rieke* with a weight average molecular weight of $M_n \approx$ 25 kg/mol. Polymer thin films were spin-coated from solution, either from a 0.6 wt % CF solution at 2000 rpm or from 1.0 wt % CB at 900 rpm. In order to enhance the smooth film formation in CB films, 10 vol % of toluene was added.

Electron microscopy was carried out using a LEO Carl Zeiss STM scanning electron microscope at an accelerating voltage of 1 kV and a working distance of 2 mm. OPV devices were prepared on prestructured and precleaned ITO substrates that were coated with a layer of PEDOT:PSS (CDT ink) at 3000

rpm. After spin-coating the active layer, an approximately 60 nm thick aluminum electrode was evaporated on top. All manufacturing steps from solution preparation to device fabrication were carried out in a nitrogen-filled glovebox. The devices were encapsulated before they were measured. The photocurrents were measured using a Keithley 237 source-measurement unit. The external quantum efficiency (EQE) spectra were obtained by illuminating the devices with a tungsten lamp (80 W) and a single-grating monochromator. The $J-V$ characteristics were recorded under simulated sunlight using a Lot Oriel solar simulator with AM1.5 at 100 mW/cm^2.

Spectroscopy. The samples for spectroscopic measurements were prepared on Spectrosil glass substrates. UV−vis measurements were carried out with a Hewlett-Packard 8453 diode array spectrometer and the fluorescence spectra with a Cary Eclipse fluorimeter. The photoluminescence quantum efficiencies (PLQE) were determined as described previously.[53] The measurements were carried out using an Ar laser at 490 nm, a nitrogen-purged integrating sphere, and a diode-array spectrometer.

The setup for TA spectroscopy has been described in detail elsewhere.[50] A 1 kHz train of 60 fs pulses (800 μJ/pulse, λ_0 = 800 nm) is split to generate pump and probe pulses using a TOPAS optical parametric amplifier and a home-built broadband noncollinear optical parametric amplifier (NOPA),[54] respectively. The effect of excitation is resolved by comparing the spectrally resolved intensity of alternate broadband probe pulses that are synchronized with excitation pulses chopped at half the frequency and referenced to the second branch of the broadband beam to mitigate the effect of shot-to-shot fluctuations. Dynamics are compiled through repeated variation of the time delay between excitation and probe pulses, which is controlled via a computer controlled mechanical delay line. After correcting for group velocity dispersion, the instrument limited time resolution is ∼120 fs, as judged by the signal rise time. In the case of TA measurements, time scales beyond nanoseconds, the second harmonic output (532 nm) of a Q-switched Nd:YVO_4 laser with 600 ps pulses was used as the excitation source and synchronized with the Ti:sapphire laser via an electronic delay generator. Samples were contained in a vacuum chamber (∼10^{-5} mbar) during TA measurements.

■ ASSOCIATED CONTENT

Supporting Information

Table showing fit parameters and figures showing $J-V$ characteristics and the BCP2-CB spectrum. This material is available free of charge via the Internet at http://pubs.acs.org.

■ AUTHOR INFORMATION

Notes

The authors declare no competing financial interest.

■ ACKNOWLEDGMENTS

J.M.H. and R.H.F. wish to acknowledge a grant from the U.K. Engineering and Physical Sciences Research Council (EPSRC). We acknowledge the financial support from the European network "PolyFilm" under RTN-6 and the German Research Council (DFG) project SPP 1355. S.H. thanks Universität Bayern e.V. for the financial support in the form of a scholarship of the Bayerische Graduiertenförderung and the Elitenetzwerk Bayern (ENB) for their support.

■ REFERENCES

(1) Buxton, G.; Clarke, N. *Phys. Rev. B* **2006**, *74*, 085207.
(2) Bates, F.; Fredrickson, G. *Annu. Rev. Phys. Chem.* **1990**, *41*, 525−557.
(3) Hamley, I. *The physics of block copolymers*; Oxford University Press: Oxford, U.K., 1998.
(4) Hoppe, H.; Sariciftci, N. S. *J. Mater. Res.* **2004**, *19*, 1924−1945.
(5) Coakley, K.; McGehee, M. *J. Chem. Mater.* **2004**, *16*, 4533−4542.
(6) Groves, C.; Marsh, R. A.; Greenham, N. C. *J. Chem. Phys.* **2008**, *129*, 114903.
(7) Lindner, S.; Hüttner, S.; Chiche, A.; Thelakkat, M.; Krausch, G. *Angew. Chem., Int. Ed.* **2006**, *45*, 3364−3368.
(8) Sommer, M.; Lindner, S.; Thelakkat, M. *Adv. Funct. Mater.* **2007**, *17*, 1493−1500.
(9) Sommer, M.; Hüttner, S.; Steiner, U.; Thelakkat, M. *Appl. Phys. Lett.* **2009**, *95*, 183308.
(10) Zhang, Q.; Cirpan, A.; Russel, T. P.; Emrick, T. *Macromolecules* **2009**, *42*, 1079−1082.
(11) Rajaram, S.; Armstrong, P. B.; Kim, B. J.; Fréchet, J. M. J. *Chem. Mater.* **2009**, *21*, 1775−1777.
(12) Campoy-Quiles, M.; Ferenczi, T.; Agostinelli, T.; Etchegoin, P. G.; Kim, Y.; Anthopoulos, T. D.; Stavrinou, P. N.; Bradley, D. D. C.; Nelson. *J. Nat. Mater.* **2008**, *7*, 158−164.
(13) Kim, Y.; Choulis, S. A.; Nelson, J.; Bradley, D. D. C.; Cook, S.; Durrant, J. R. *Appl. Phys. Lett.* **2005**, *86*, 063502.
(14) Ma, W.; Yang, C.; Gong, X.; Lee, K.; Heeger, A. *Adv. Funct. Mater.* **2005**, *15*, 1617−1622.
(15) Chang, J. F.; Sun, B. Q.; Breiby, D. W.; Nielsen, M. M.; Sölling, T. I.; Giles, M.; McCulloch, I.; Sirringhaus, H. *Chem. Mater.* **2004**, *16*, 4772−4776.
(16) Kline, R. J.; McGehee, M. D.; Kadnikova, E. N.; Liu, J.; Fréchet, J. M. J.; Toney, M. F. *Macromolecules* **2005**, *38*, 3312−3319.
(17) Chesterfield, R. J.; McKeen, J. C.; Newman, C. R.; Ewbank, P. C.; Filho, D. A. D.; Brédas, J.; Miller, L. L.; Mann, K. R.; Frisbie, C. D. *J. Phys. Chem. B* **2004**, *108*, 19281−19292.
(18) Tatemichi, S.; Ichikawa, M.; Koyama, T.; Taniguchi, Y. *Appl. Phys. Lett.* **2006**, *89*, 112108.
(19) Hüttner, S.; Sommer, M.; Thelakkat, M. *Appl. Phys. Lett.* **2008**, *92*, 093302.
(20) Dittmer, J. J.; Marseglia, E. A.; Friend, R. H. *Adv. Mater.* **2000**, *12*, 1270−1274.
(21) Shoaee, S.; An, Z.; Zhang, X.; Barlow, S.; Marder, S. R.; Duffy, W.; Heeney, M.; McCulloch, I.; Durrant, J. R. *Chem. Commun.* **2009**, 5445−5447.
(22) Keivanidis, P. E.; Howard, I. A.; Friend, R. H. *Adv. Funct. Mater.* **2008**, *18*, 3189−3202.
(23) Foster, S.; Finlayson, C. E.; Keivanidis, P. E.; Huang, Y.-S.; Hwang, I; Friend, R. H.; Otten, M. B. J.; Lu, L.-P.; Schwartz, E.; Nolte, R. J. M.; Rowan, A. E. *Macromolecules* **2009**, *42*, 2023−2030.
(24) Zhou, E.; Cong, J.; Wei, Q.; Tajima, K.; Yang, C.; Hashimoto, K. *Angew. Chem., Int. Ed.* **2011**, *50*, 2799−2803.
(25) Green, M. A.; Emery, K.; Hishikawa, Y.; Warta, W. *Prog. Photovoltaics* **2011**, *19*, 84−92.
(26) Sommer, M.; Huettner, S.; Thelakkat, M. *J. Mater. Chem.* **2010**, *20*, 10788−10797.
(27) Olsen, B. D.; Segalman, R. A. *Mater. Sci. Eng.* **2008**, *62*, 37−66.
(28) Huang, Y. S.; Westenhoff, S.; Avilov, I.; Sreearunothai, P.; Hodgkiss, J. M.; Deleener, C.; Friend, R. H.; Beljonne, D. *Nat. Mater.* **2008**, *7*, 483−489.
(29) Sommer, M.; Lang, A. S.; Thelakkat, M. *Angew. Chem., Int. Ed.* **2008**, *47*, 7901−7904.
(30) Wu, Z.; Petzold, A.; Henze, T.; Thurn-Albrecht, T.; Lohwasser, R.; Sommer, M.; Thelakkat, M. *Macromolecules* **2010**, *43*, 4646−4653.
(31) Clark, J.; Silva, C.; Friend, R. H.; Spano, F. C. *Phys. Rev. Lett.* **2007**, *98*, 206406.
(32) Hoffmann, M.; Schmidt, K.; Fritz, T.; Hasche, T.; Agranovich, V.; Leo, K. *Chem. Phys.* **2000**, *258*, 73−96.

(33) Hüttner, S.; Sommer, M.; Hodgkiss, J.; Kohn, P.; Thurn-Albrecht, T.; Friend, R. H.; Steiner, U.; Thelakkat, M. *ACS Nano* **2011**, *5*, 3506−3515.
(34) McNeill, C. R.; Abrusci, A.; Hwang, I.; Ruderer, M. A.; Müller-Buschbaum, P.; Greenham, N. C. *Adv. Funct. Mater.* **2009**, *19*, 3103−3111.
(35) Cook, S.; Furube, A.; Katoh, R. *Energy Environ. Sci.* **2008**, *1*, 294−299.
(36) Campbell, A. R.; Hodgkiss, J. M.; Westenhoff, S.; Howard, I. A.; Marsh, R. A.; McNeill, C. R.; Friend, R. H.; Greenham, N. C. *Nano Lett.* **2008**, *8*, 3942−3947.
(37) Marsh, R. A.; McNeill, C. R.; Abrusci, A.; Campbell, A. R.; Friend, R. H. *Nano Lett.* **2008**, *8*, 1393−1398.
(38) Marks, R.; Halls, J.; Bradley, D.; Friend, R.; Holmes, A. *J. Phys.: Condens. Mater* **1994**, *6*, 1379−1394.
(39) Murgatroyd, P. N. *J. Phys. D* **1970**, *3*, 151.
(40) Zhokhavets, U.; Erb, T.; Hoppe, H.; Gobsch, G.; Sariciftci, N. *Thin Solid Films* **2006**, *496*, 679−682.
(41) Yago, T.; Tamaki, Y.; Furube, A.; Katoh, R. *Phys. Chem. Chem. Phys.* **2008**, *10*, 4435−4441.
(42) Howard, I. A.; Laquai, F.; Keivanidis, P. E.; Friend, R. H.; Greenham, N. C. *J. Phys. Chem. C* **2009**, *113*, 21225−21232.
(43) Marsh, R. A.; Hodgkiss, J. M.; Albert-Seifried, A.; Friend, R. H. *Nano Lett.* **2010**, *10*, 923−930.
(44) Westenhoff, S; Howard, I. A.; Hodgkiss, J. M.; Kirov, K. R.; Bronstein, H. A.; Williams, C. K.; Greenham, N. C.; Friend, R. H *J. Am. Chem. Soc.* **2008**, *130*, 13653−13658.
(45) Ford, T. A.; Avilov, I.; Beljonne, D.; Greenham, N. C. *Phys. Rev. B* **2005**, *71*, 125212.
(46) Ohkita, H.; Cook, S.; Astuti, Y.; Duffy, W.; Heeney, M.; Tierney, S.; McCulloch, I.; Bradley, D. D. C.; Durrant, J. R. *Chem. Commun* **2006**, *37*, 3939−3941.
(47) Assuming 0.3 eV exciton binding energy and based on 1.9 eV singlet excited state energy for P3HT as well as an interfacial charge transfer energy of 1.3 eV (see Figure 1).
(48) Sakurai, K.; Tachibana, H.; Shiga, N.; Terakura, C.; Matsumato, M.; Tokura, Y. *Phys. Rev. B* **1997**, *56*, 9552−9556.
(49) Köhler, A.; Blejonne, D. *Adv. Funct. Mater.* **2004**, *14*, 11−18.
(50) Hodgkiss, J. M.; Tu, G.; Albert-Seifried, S.; Huck, W. T. S.; Friend, R. H. *J. Am. Chem. Soc.* **2009**, *131*, 8913−892.
(51) Hodgkiss, J. M.; Campbell, A. R.; Marsh, R. A.; Rao, A.; Albert-Seifried, S.; Friend, R. H. *Phys. Rev. Lett.* **2010**, *104*, 177701.
(52) Ryan, A. J. *Nat. Mater.* **2002**, *1*, 8−10.
(53) deMello, J. C.; Wittmann, H. F.; Friend, R. H. *Adv. Mater.* **1997**, *9*, 230−232.
(54) Laquai, F.; Mishra, A. K.; Müllen, K.; Friend, R. H. *Adv. Funct. Mater.* **2008**, *18*, 1−11.